The Meteoritical Society

Meteoritics & Planetary Science 1–13 (2015)
doi: 10.1111/maps.12498

Organic and inorganic correlations for Northwest Africa 852 by synchrotron-based Fourier transform infrared microspectroscopy

Mehmet YESILTAS[1], Robert E. PEALE[1*], Miriam UNGER[2], Julia SEDLMAIR[3], and Carol J. HIRSCHMUGL[2]

[1]Department of Physics, University of Central Florida, Orlando, Florida 32816, USA
[2]Department of Physics, University of Wisconsin-Milwaukee, Milwaukee, Wisconsin 53211, USA
[3]Forest Products Laboratory, US Department of Agriculture Forest Service, Madison, Wisconsin 53726, USA
[*]Corresponding author. E-mail: robert.peale@ucf.edu

(Received 13 November 2013; revision accepted 10 July 2015)

Abstract–Relationships between organic molecules and inorganic minerals are investigated in a single 34 μm diameter grain of the CR2 chondrite Northwest Africa 852 (NWA) 852 with submicron spatial resolution using synchrotron-based imaging micro-FTIR spectroscopy. Correlations based on absorption strength for the various constituents are determined using statistical correlation analysis. The silicate band is found to be correlated with the hydration band, and the latter is highly correlated with stretching modes of aliphatic hydrocarbons. Spatial distribution maps show that water+organic combination, silicate, OH, and C-H distributions overlap, suggesting a possible catalytic role of phyllosilicates in the formation of organics. In contrast, the carbonate band is anticorrelated with water+organic combination, however uncorrelated with any other spectral feature. The average ratio of asymmetric CH_2 and CH_3 band strengths (CH_2/CH_3 = 2.53) for NWA 852 is similar to the average ratio of interplanetary dust particles (~2.40) and Wild 2 cometary dust particles (2.50), but it significantly exceeds that of interstellar medium objects (~1.00) and several aqueously altered carbonaceous chondrites (~1.40). This suggests organics of similar length/branching, and perhaps similar formation regions, for NWA 852, Wild 2 dust particles, and interplanetary dust particles. The heterogeneous spatial distribution of ratio values indicates the presence of a mixture of aliphatic organic material with different length/branching, and thus a wide range of parent body processes, which occurred before the considered grain was formed.

INTRODUCTION

Carbonaceous chondrites are the most primitive meteorites (Cloutis et al. 2012) and are probably fragments of primitive asteroids or comets (Anders 1975). Some carbonaceous chondrites are aqueously altered to a greater or lesser extent (petrologic types 1 and 2, respectively), while others are thermally metamorphosed (types 3–6) (Huss et al. 2006). These meteorites still carry records of presolar material as well as solar nebula and postaccretion processes. The organic carbon content of CI, CM, and CR chondrites amounts to at least ~4 wt% (Orthous-Daunay et al. 2013), and they contain higher concentrations and varieties of organic molecules than other meteorite types (Sephton 2002). Although Tagish Lake has the highest carbon content (as high as 6 wt%), its organic fraction is only 2.6 wt% (Brown et al. 2000).

In some cases, organic matter of interstellar origin survived processing and remained intact within meteorite parent bodies (Martins 2011). Some species may arise during alterations (Sephton et al. 1998, 2003), e.g., melting of ices would hydrate simple organic molecules, producing organic compounds of higher complexity. Delivery of these complex prebiotic organic compounds may have contributed to the origin of life on early Earth (Chyba and Sagan 1992; Owen and Bar-Nun 1995; Morbidelli et al. 2000; Campins et al. 2010;

Rivkin and Emery 2010; Licandro et al. 2011). Understanding how organic compounds are formed in extraterrestrial matter is therefore important to the question of how life arose on Earth (Ponnamperuma et al. 1982). Relationships between organic matter and mineral species may provide clues to such formation; however, little is known about the spatial distribution and mineralogical relationships of organics in meteorites.

Catalytic surfaces (e.g., mineral surfaces) are necessary for the production of organic matter (Cleaves et al. 2012). The nature and characteristics of mineral surfaces affect reaction rates, so that particular organic molecules may be preferentially concentrated on particular mineral surfaces (Lahav and Chang 1976; Rode et al. 1999; Desaubry et al. 2003). Therefore, a genetic link between organic matter and mineral products of aqueous alteration such as phyllosilicates is highly possible. Evidence is that carbonaceous chondrites with abundant aqueous alteration product minerals (CI and CM chondrites) are also significantly rich in organic matter (Pearson et al. 2002). Relationships between organic matter (of unknown nature) and aqueous alteration were recently reported by Le Guillou and Brearley (2014). However, relationships between specific minerals and specific molecules within meteorites remain poorly understood. Complex organic synthesis has been linked with minerals (Ponnamperuma et al. 1982; Pearson et al. 2002), but the actual mineral species and crystalline phases involved are still in question.

Northwest Africa 852 (NWA 852) is a CR2 carbonaceous chondrite with low weathering grade (W1), 1.3 Fa (mole%), and 4.3 Fs (mole%) (Russell et al. 2002). It reportedly presents low chondrules/matrix ratio and Fe-rich olivines (Russell et al. 2002). Furthermore, NWA 852 presents high presolar grain abundances. Leitner et al. (2012) reported 24 presolar silicates (78 ppm), 7 presolar oxides (38 ppm), and 8 SiC grains (~160 ppm) in NWA 852. The latter value is considered by those authors as the highest known in primitive meteorites. However, to date no study exists on organic and mineral inventory of NWA 852.

Organic molecules and minerals have characteristic vibrational absorption lines in the midinfrared between 3 and 15 μm wavelengths, which is an important region for remote characterization of cosmic dust and meteorite source objects (e.g., Beck et al. 2010; Vernazza et al. 2010). Here we report, for the first time, synchrotron-based Fourier transform infrared microspectroscopy (micro-FTIR) of NWA 852 in the midinfrared region. This analytical technique gives information on the organic and inorganic content in single meteorite grains with submicron spatial resolution. Relationships between organics and minerals are studied in situ without chemical extraction. Grain heterogeneity and correlations between different spectral features are revealed for NWA 852. Preliminary data from this work were reported in Yesiltas et al. (2013a, 2013b).

SAMPLE AND EXPERIMENTAL DETAILS

Four pieces of NWA 852 were recovered from Sahara desert, Morocco in 2001, totaling to 174 g. A ~50 mg chip of NWA 852 was obtained from Prof. Daniel Britt and was ground to ~30 micron-sized powders with an agate mortar and pestle. After dozens of similar grinding operations, we observed fine scratches on the bottom of the mortar, which may have added agate grains as impurities in the mixture of meteorite grains. Agate has a hardness of up to 7 on the Mohs scale, so evidently there are harder grains in NWA852. However, infrared spectra of such agate impurity grains would show only the silicate band. We do not believe that scratching of the hard agate could result in a film of contamination that would stick to individual meteorite grains, thus contaminating their infrared spectra. We note that grinding in an agate mortar is common and accepted practice in meteoritics.

A sparse layer of nonoverlapping grains was placed on a diamond window for micro-FTIR transmittance spectroscopy. Spectra of individual grains were collected after regions of interest were defined under the optical microscope. This paper presents data on a single 34 μm diameter grain to illustrate the technique for investigating the mineral–organic relations in meteorites in situ.

Contamination and terrestrial weathering can affect meteorites and alter their spectra (e.g., Botta and Bada 2002). NWA 852 itself has experienced very little terrestrial weathering and is classified as weathering grade W1 (Leitner et al. 2012). The C-H stretching region near 3000–2800 cm^{-1} is especially susceptible to contamination. For instance, it was reported by Kebukawa et al. (2009) that storing meteorite samples in containers which include silicone rubber, silicone grease, or adhesive tape contaminated the samples within very short times with volatile organics. Our sample handling is free of any of these materials. After grinding, we stored our meteorite samples in a weighing paper, which is water and air resistant, and no evidence of contamination was observed. In particular, several other carbonaceous chondrites were stored and prepared in the same way as NWA 852, but these show very much weaker CH stretching features. Therefore, the much stronger features we see in NWA 852 cannot have arisen from contamination due to our sample preparation protocol.

The experiment was installed on the IRENI (Infrared Environmental Imaging) beam line at the (now-closed) Synchrotron Radiation Center (SRC), University of Wisconsin, Madison. Multiple fans of radiation extracted from a bending magnet were collimated, and rearranged with mirrors into a 3 × 4 matrix of beams, which homogeneously illuminates the 34 μm × 34 μm field of view used here. The end station of the beam line is a Bruker Vertex 70 interferometer connected to a Bruker Hyperion IR microscope equipped with a Focal Plane Array (FPA) detector of 3850–900 cm^{-1} spectral range (2.5–12.5 μm). The microscope operated in transmission mode with a 74×, 0.6 NA, Schwarzschild–Cassegrain objective and a 20×, 0.6 NA condenser. The geometric effective area at the sample plane of 0.54 μm × 0.54 μm pixels imaged onto 40 μm × 40 μm pixels at the detector allows spatial oversampling, providing spatially resolved images that are diffraction-limited at all wavelengths. The single shot FPA image covers the field of view with 96 × 96 pixels. A detailed review of the beamline is presented in Hirschmugl and Gough (2012). The sample to be analyzed was placed on a diamond window which was mounted onto a motorized, programmable mapping stage. After having defined the mapping parameters, infrared spectra from all pixels within the defined area were simultaneously collected within minutes. These raw spectra were later divided by reference spectra collected at a sample-free region of the diamond substrate to obtain transmittance.

Using commercial IGOR Pro and IRidys software packages (Nasse et al. 2011), a spatially averaged IR spectrum of the grain was obtained by masking out the sample-free regions of the image and averaging the spectra for all pixels in the unmasked region. The same software also allowed us to obtain line profiles across the meteorite grain by extracting individual spectra from adjacent pixels. The integrated absorbance of individual characteristic spectral features was taken as a measure of the relative concentrations of specific minerals and organics at a particular location within the grain. Correlation coefficients were obtained using the descriptive statistics function of the OriginPro software package. Integrated intensity maps were generated and used to obtain the spatial distribution of the various mineral and organic types within the grain.

RESULTS

IR Spectral Signatures

Figure 1 presents the infrared image of the investigated NWA 852 grain at 2920 cm^{-1} wave numbers. This wave number corresponds to the CH stretch band of CH_2 moieties in aliphatic hydrocarbons. The grain nearly fills a 34 μm × 34 μm field of view, which contains ~3964 pixels. A separate infrared spectrum is collected for each pixel. The vertical line indicates a slice through the grain, and the cross ticks on this line identify the positions where individual spectra were collected, plotted, and analyzed below.

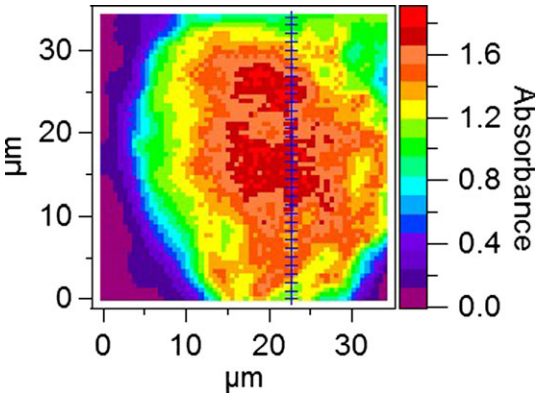

Fig. 1. Infrared image of the investigated NWA 852 grain at 2921 cm^{-1} wavenumbers. The 16 level color scale in rainbow sequence indicates absorbance values, red being the highest. The vertical cut defines a profile through the grain and the positions (ticks) where individual spectra were selected for plotting and analysis.

Figure 2 presents the spatially averaged midinfrared spectrum of the same grain. Lettered arrows indicate the position of distinct and identifiable absorbance bands due to specific vibrational modes. Assignments are given in the Fig. 2 caption and in Table 1. Although the peak of the G band is fairly flat, this band is not saturated in any of our data. The pixel with the strongest G band had peak absorbance before baseline subtraction of 1.85, so that no spectrum had less than 15.7% transmittance at any wave number. Broad and flat G bands are widely reported in the meteorite literature, even for very weak absorbance values (Raynal et al. 2000; Kebukawa et al. 2011; Briani et al. 2013).

The symmetric band A near 1018 cm^{-1} is due to the Si-O stretching vibrational modes in silicates (Matrajt et al. 2004; Merouane et al. 2012). The broad band G near 3400 cm^{-1} is due to stretching mode of interlayer and/or adsorbed water (Kebukawa et al. 2010a). Together the A and G bands indicate the presence of hydrous silicates, possibly clay minerals, in this meteorite sample. This is consistent with the identification of clay in CR2 chondrites (e.g., Morlok and Libourel 2013). On the other hand, the signature band of structural OH near 3650 cm^{-1}, as would be observed in some phyllosilicates, and which we have observed for grains of Orgueil and Tagish Lake by the same technique (Yesiltas, unpublished data), is absent in this spectrum. The asymmetric band labeled B is mostly due to carbonates (e.g., Matrajt et al. 2004; Kebukawa et al. 2010a; Merouane et al. 2012; Sandford et al. 2013).

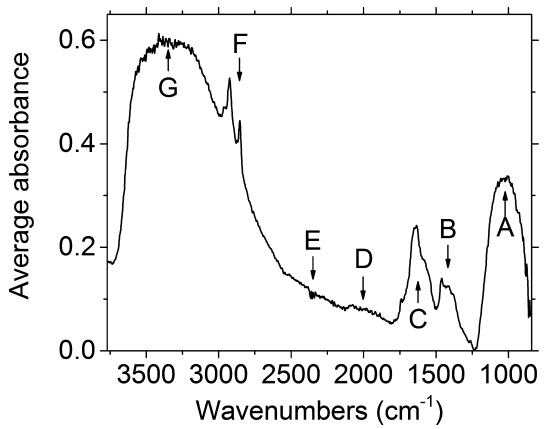

Fig. 2. Spatially averaged absorbance spectrum of the NWA 852 grain shown in Fig. 1. Letters indicate absorbance bands due to specific vibrational modes. Assignments (Table 1) are A: silicates; B: carbonates; C: water/organics; D: water/silicate overtones; E: artifact from atmospheric CO_2; F: aliphatic hydrocarbons; G: OH due to interlayer/adsorbed water.

Table 1. Positions and interpretation of the observed bands.

Label	Band center (cm^{-1})	Mode	Assignments
A	1018	Si-O stretch[a]	Phyllosilicates
B	1411	C=O stretch	Carbonates
C	1650/1730	H-O-H bend[d,e]/ C=O stretch[a,b,c]	Phyllosilicates/ organics
D	2000	H-O-H[d]	Water/silicate overtones
E	2300	C=O	Atmospheric CO_2
F	2800–3000	C-H stretch[a,d,e]	Aliphatic hydrocarbons
G	3400	H-O-H stretch[f]	Interlayer/adsorbed water

[a]Matrajt et al. (2004).
[b]Orthous-Daunay et al. (2013).
[c]Kebukawa et al. (2011).
[d]Raynal et al. (2000).
[e]Kebukawa et al. (2010b).
[f]Kebukawa et al. (2010a).

The broad band C in Fig. 2 is a combination of H-O-H bending modes in water (Raynal et al. 2000; Kebukawa et al. 2010a) and modes of organics such as aromatics (e.g., Nakamura et al. 2003a, 2003b; Matrajt et al. 2004) and carbonyls (Kebukawa et al. 2011; Orthous-Daunay et al. 2013). Sharp and distinct absorbance lines in the range 2800–3000 cm^{-1} comprising band F are C-H stretching modes due to aliphatic hydrocarbons (Raynal et al. 2000; Matrajt et al. 2004; Kebukawa et al. 2010b). Figure 2 lacks evidence for the CH stretch of aromatic hydrocarbons, which would appear above 3000 cm^{-1}.

A weak broad band D is observed in Fig. 2 between 1800 and 2130 cm^{-1}. This band may be due to bound and free H_2O (Raynal et al. 2000) or overtones of silicates. Narrow spikes labeled "E" near 2360 cm^{-1} are artifacts due to atmospheric CO_2. Table 1 collects these observed absorbance bands as well as their positions and interpretations.

Spectral Profile of the Grain

A spectroscopic line profile across the grain is obtained for the slice indicated by the vertical line on the infrared image in Fig. 1. This profile consists of 63 pixels, each with an associated spectrum. Alternate pixels were selected for data analysis with 1 μm separation. The 33 spectra are presented in Fig. 3 with the ordering of the curves bottom to top following a bottom to top scan across the grain (Fig. 1). For each spectrum in Fig. 3, the integrated absorbance of characteristic bands was determined by calculating the area under the curve and above a linear baseline that connected the end points of the integration range. For the case of the partially overlapping bands B and C, the line connecting the high end of band C with the low end of band B was taken as their common baseline for their integrations. The shaded boxes in Fig. 3 indicate those curves for which the integrated absorbance exceeds the median integrated absorbance. The widths of the shaded boxes indicate the integration ranges. The spectral integration limits were 850–1200, 1250–1500, 1500–1750, 2800–3000, and 3000–3700 cm^{-1} for bands A, B, C, F, and G, respectively. The boxes suggest good spatial overlap for bands A, C, F, and G, i.e., between silicates, OH, and organics. The spatial distribution for carbonates (B) seems quite different.

Figure 4 compares integrated absorbances of bands A, B, C, F, and G as a function of position along the slice indicated in the IR image Fig. 1. The lower axis gives the pixel number, while the upper axis indicates the physical location where the spectrum was collected along the slice from the bottom of the grain to the top. The integrated absorbance of the various bands changes with position along the slice through the grain. The spatial variations in the absorbance are different for different bands. Absorbance is the product of absorption cross section, concentration, and thickness (i.e., photon path length through the grain). If the changes were due simply to the nonuniform thickness of the grain, then all of the absorbances would change together. The absorption cross section is constant for a given band, independent of position. Thus, the different spatial dependences for the different bands indicate different spatial distributions of the responsible minerals

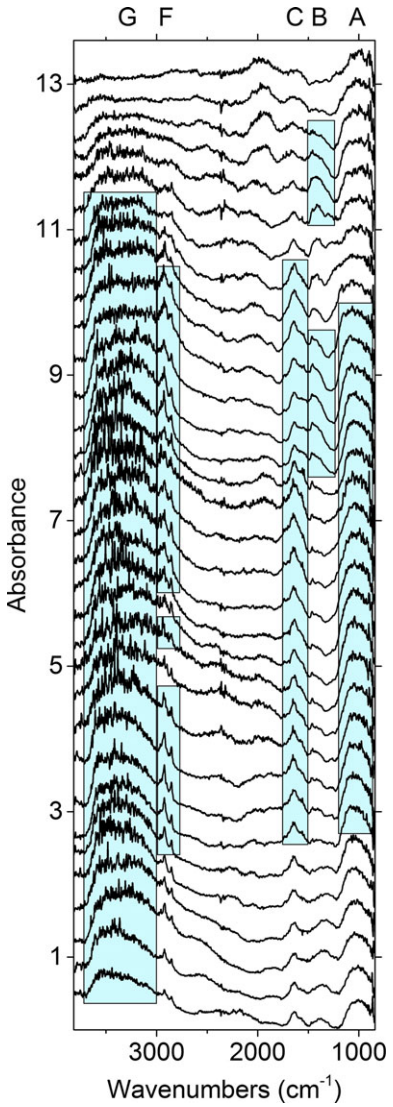

Fig. 3. Spectral line scan for cut indicated in Fig. 1. Each successive spectrum is offset vertically by 0.4 absorbance units for clarity. Shaded boxes group spectra whose integrated absorbance within the box horizontal range exceeds the median.

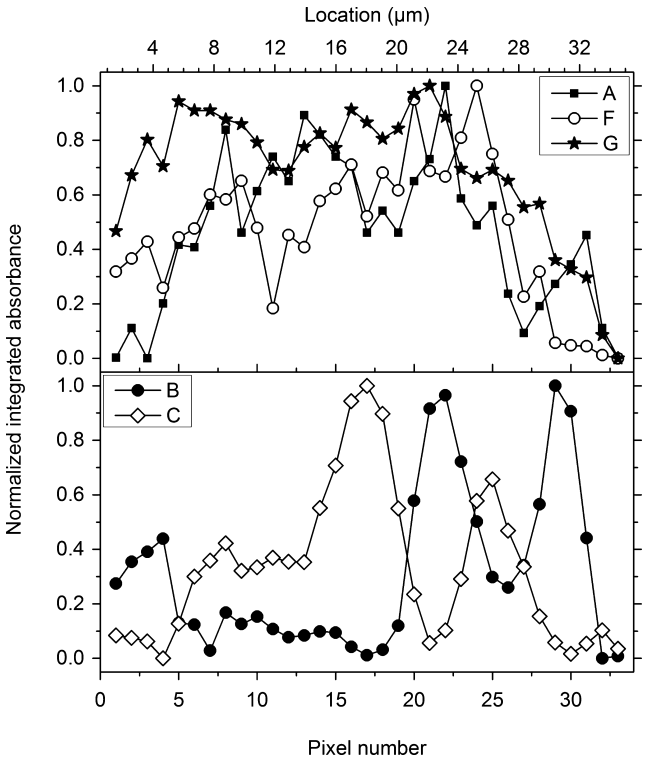

Fig. 4. Normalized integrated absorbance of bands A-G as a function of position along the slice indicated in the IR image Fig. 1. The lower axis gives the pixel number, while the upper axis indicates the physical location where the spectrum was collected along the slice from the bottom of the grain to the top.

and molecules. In Fig. 4, the strongest correlation is the evident *anti*correlation of bands B and C.

Correlation Coefficients

We employed Pearson's correlation method to quantify correlations between absorbance bands observed in spectra of NWA 852. Pearson's method determines relationships among variables in a data set, e.g., Hopkins (1978). We let X represent the integrated absorbance of one of the bands and let Y be the same for one of the other bands. The variance S_x^2 of X is calculated from

$$S_x^2 = \frac{\sum(X-\bar{X})(X-\bar{X})}{n-1} \quad (1)$$

Equation 1 is positive definite. The covariance (S_{xy}) is then calculated from

$$S_{xy} = \frac{\sum(X-\bar{X})(Y-\bar{Y})}{n-1} \quad (2)$$

Equation 2 may be positive or negative. For example, if at a given pixel the value of X exceeds its value averaged over all pixels, while the value of Y is less than its average, then at that pixel the argument of the sum is negative. We obtain S_{xy} by summing over all pixels, and if this sum is negative, then on average the X values exceed their average when the Y values are below theirs, and vice versa. Finally, by normalizing with Equation 1, we obtain the correlation coefficient as

$$r = \frac{S_{xy}}{S_x S_y} \quad (3)$$

The values of r lie between -1 and $+1$. Negative values indicate anticorrelation and positive values

Table 2. Correlation coefficients. Letters represent the absorbance bands in Fig. 2.

		(A)	(B)	(C)	(F)	(G)
(A)	Corr.	1	0.01	0.41*	0.54*	0.59*
	Sig.	–	0.96	0.01	0.01	3.02×10^{-4}
(B)	Corr.		1	−0.51*	0.01	−0.08
	Sig.		–	0.01	0.98	0.66
(C)	Corr.			1	0.54*	0.42*
	Sig.			–	0.01	0.01
(F)	Corr.				1	0.76*
	Sig.				–	3.38×10^{-7}
(G)	Corr.					1
	Sig.					–

(A) Silicates; (B) carbonates; (C) H_2O+organics; (F) aliphatic hydrocarbons; (G) OH. * Indicates the correlation is significant at the 95% confidence level.

indicate positive correlation. The closer a coefficient is to ±1, the stronger is the correlation or anticorrelation.

The integrated intensities determined as for Figures 3 and 4 comprise our data set for correlation analysis. A caution is appropriate here, as the physically interesting spatial correlations are those of concentration, while we calculate those of absorbance, which depends on sample thickness. It is easy to show from Equations 1–3 for a hypothetical sample with just two regions that a positive spatial correlation of concentration can be turned into a negative correlation of absorbance if the sample thickness and mineral concentration change oppositely, and if the ratio of the thicknesses is within a certain range. However, our correlation analysis sums over 33 positions. For a positive correlation in absorbances to be due only to thickness variations would require concentrations to change in going from one point to another mainly oppositely to the thickness changes. This would be an unlikely coincidence.

Based on the integrated absorbances, correlation coefficients as well as their respective significance levels were calculated and collected in Table 2. Coefficients with "*" indicate those correlations are significant at the 95% confidence level. In other words, possibility of a correlation being due to chance is 5% or less. The "strengths" of correlations are determined according to the scale known as "Cohen's rule," namely 0.1–0.3 is "weak," 0.3–0.5 is "medium," and 0.5–1.0 is "strong" (Cohen 1988).

We observe that the two bands F and C associated with hydrocarbons unsurprisingly show strong correlation ($r = 0.54$). Band A (silicates) is strongly correlated ($r = 0.59$) with band G (OH band), suggesting significant concentration of phyllosilicates throughout the grain. Organic bands C and F are strongly correlated with silicates band A. The aliphatic hydrocarbon band F is quite strongly correlated with the OH band G, but the correlation of C and G is moderate. This suggests that band C is composed more of organics than of water, as water and OH would be strongly correlated. Band B (carbonates) shows strong negative correlation with band C, corresponding to the anticorrelation between them already noted in Fig. 4.

Spatial Distribution of Organic and Mineral Compounds

Infrared images give the spatial distribution of absorbance at a particular wave number. Such maps may be used to infer the relative amounts of organic matter or inorganic minerals present at particular locations within a grain. Our high spatial resolution, broad spectral coverage, and simultaneous data acquisition over the entire field of view allow us to acquire detailed spatial maps of composition for many grains in short times. These maps are obtained by integrating the infrared image (Fig. 1) over the frequency range of the spectral band of interest. Figure 5 presents these integrated absorbance maps of the NWA 852 grain for the absorbance bands A, B, C, F, G. The method and spectral range of integration is the same as for Figs. 3 and 4.

Figure 5A indicates that silicates are distributed across the grain. The highest absorbance comes from the central region, presumably where the grain is thicker, around the coordinates (20 μm, 20 μm). Figure 4G presents the spatial distribution for OH, which also has prominent absorption in the region near (20 μm, 20 μm). The spectral overlap for these two maps is less in other spatial regions, e.g., in the upper right corner of the grain where A shows strong absorption lacking in G. Thus, the region near (20 μm, 20 μm) may have abundant hydrous silicates (e.g., phyllosilicates), while the other regions of strong absorption in Fig. 5A may correspond to anhydrous silicates (e.g., olivine, pyroxene). Note that the olivine shoulders at 873, 925, and 956 cm^{-1} are within the band A integration range.

Spatial distribution of carbonates is presented in Fig. 5B. This map shows presence of high carbonate concentration along the outer edges of the grain and little within the center. In particular, the overlap of carbonates with silicates (A), OH (G), or organics (F) is weak. That the Pearson coefficients do not show strong negative correlation between band B and bands A, G, and F is a sampling effect, as few points on the rim of the grain were included in the analysis.

Figure 5C presents the map of absorbance due to organic–water combination. Some of the structure in the spatial distribution seems similar to that of carbonates. This may be an artifact as the partial

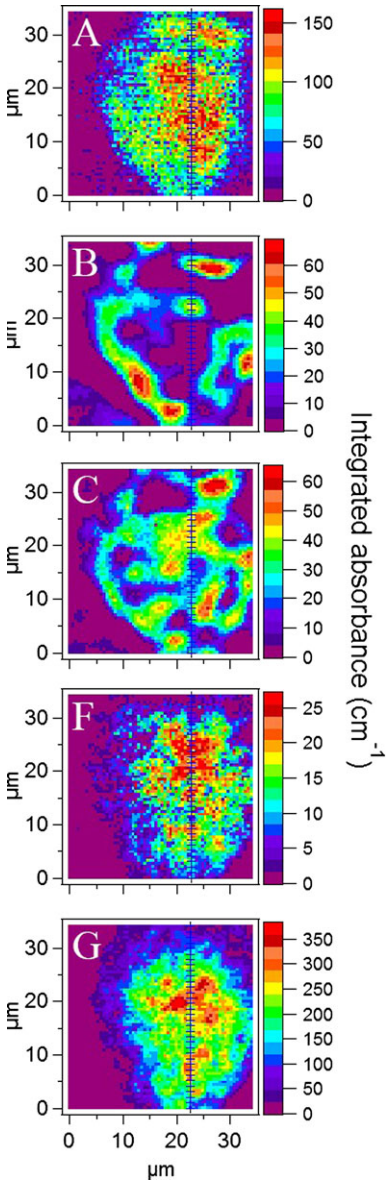

Fig. 5. Integration maps of NWA 852 grain for characteristic absorbance features. A) Silicates; B) carbonates; C) organics and water; F) aliphatic hydrocarbons; G) OH due to interlayer/adsorbed water. The color scale in rainbow sequence indicates the integrated absorbance values in 16 levels, red being the highest.

spectral overlap of bands B and C make their integrals somewhat interdependent. However, the islands of strongest B and C absorbance appear spatially distinct. Kebukawa et al. (2010a) showed that organics and water tend to be interleaved with carbonate regions in Bells.

The spatial distribution map for aliphatic hydrocarbons (F) overlaps more with OH (G) than with silicates (A). This agrees with the correlation coefficients 0.76 and 0.54, respectively, for the line profile.

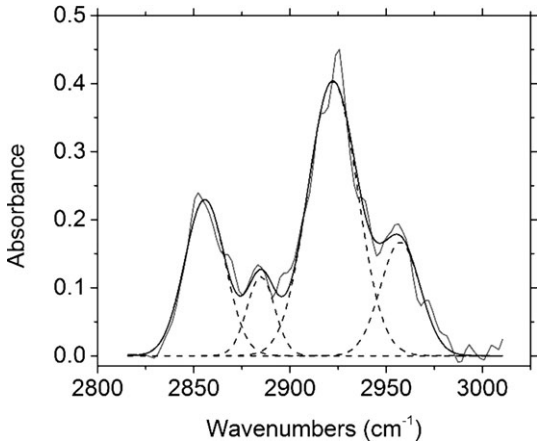

Fig. 6. Baseline subtracted F-band and Gaussian fit.

Moreover, it is consistent with the reported association of organics and phyllosilicates (e.g., Pearson et al. 2002; Kebukawa et al. 2010a).

CH_2/CH_3 Ratios

Aliphatic hydrocarbons give rise (Fig. 2) to infrared features between 2800 and 3000 cm^{-1} due to C-H stretching vibrational modes. Features at 2850 and at 2921 cm^{-1} are attributed to CH stretches arising from CH_2 moieties, such as occur in the middle of aliphatic chains. Features at 2875 and 2960 cm^{-1} are attributed to CH stretches arising from CH_3 moieties, such as occur at the free ends of aliphatic chains. Branched aliphatic hydrocarbons will have more free ends and a higher proportion of CH_3 moieties. Thus, aliphatic chain length and degree of branching can be inferred from the CH_2/CH_3 absorbance ratios (Marshall et al. 2005; Igisu et al. 2009; Kebukawa et al. 2010a). A low ratio suggests that the chain lengths of aliphatic content were shortened by some process, such as impacts of energetic particles. Such processing makes the body less primitive. The longer aliphatic chains and/or low branching inferred from a high CH_2/CH_3 ratio suggest less processing and hence more primitive (or pristine) material (Matrajt et al. 2013).

We performed a Gaussian-fitting procedure to 30 pixels selected from the organic-rich part of the grain with strong F bands, having integrated absorbance of at least 18 cm^{-1}. First, we baseline corrected band F by subtracting the straight line that connects the end points of that region at 2800 and 3000 cm^{-1}. The SNR, defined as the F band peak height relative to the noise, was 3 for the worst spectra considered and 25 for the best. CH_2/CH_3 ratios were determined from the integrated areas of the fits. Uncertainties were defined mainly by choice of baseline to be subtracted and not by the noise. An example spectrum with fitted Gaussian peaks is presented in Fig. 6, where integrated area is

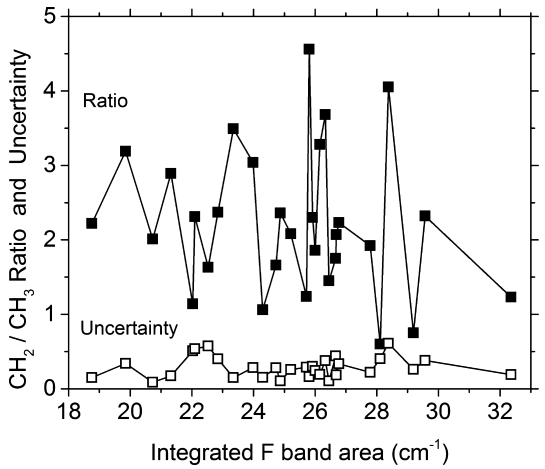

Fig. 7. Distribution of ratios and their uncertainties as a function of integrated F-band area.

~25 cm^{-1} and SNR is about 10. This fitting procedure yields an absorbance residue of ±0.02 (difference between fit and data), which is comparable to values for published studies (e.g., Orthous-Daunay et al. 2013). The residue on the spectrum with the worst SNR considered was ±0.035.

CH_2/CH_3 ratios and their uncertainties are plotted as a function of integrated band strength in Fig. 7. There may be a slight tendency for the ratio to decrease with increasing band strength, but the uncertainty shows no significant trend. Furthermore, uncertainty appears to be uncorrelated with ratio. The uncertainties in all cases are much less than the values of the ratios, and they are also much less than the variation in ratio values. Thus, ratio values as low as 1.5 and as high as 4 are significant, indicating that NWA 852 contains a mixture of both lightly and heavily processed organic material. This suggests a wide range of parent body processes, which must have occurred before the considered grain was formed.

Figure 8 presents the histogram of the ratios. While the distribution of the ratios in the small sample considered is useful to demonstrate the range of ratio values that occur at high spatial resolution, the grain average is also interesting. For this, we consider the ratio for the grain averaged spectrum plotted in Fig. 2, where the SNR is much higher than for any individual pixel's spectrum. This analysis gives the ratio 2.53, which is compared in Table 3 to values reported for other meteorites, interplanetary dust particles (IDPs), diffuse interstellar medium (DISM) objects, and cometary dust particles. The value for NWA 852 is similar to that of IDPs and Wild 2 cometary dust particles. It exceeds those of DISM and several carbonaceous chondrites of petrologic type 1 and 2.

Table 3. Astronomical objects and their CH_2/CH_3 ratios.

Objects	I_{CH2}/I_{CH3}
Sutter's Mill (SM2)	4.00[h]
NWA 852 (CR2)	2.53[a]
Wild 2 particles	2.50[b]
IDPs (anhydrous)	2.46[c,i]
Sutter's Mill (SM12)	2.44[h]
IDPs (hydrous)	2.31[c,i]
Paris (CM)	1.80[g]
Bells (CM2)	1.40[f]
Orgueil (CI1)	1.40[f]
DISM	1.17[d,i], 1.07[e,i]
Murchison (CM2)	1.00[f]

[a]This study.
[b]Keller et al. (2006).
[c]Flynn et al. (2003).
[d]Sandford et al. (1991).
[e]Pendleton et al. (1994).
[f]Kebukawa et al. (2010a).
[g]Merouane et al. (2012).
[h]Yesiltas et al. (2014).
[i]Average.

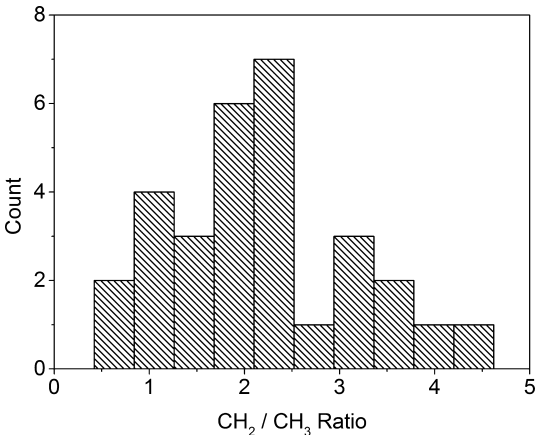

Fig. 8. Histogram of the CH_2/CH_3 ratios for 31 pixels.

DISCUSSION

Investigation of organic molecule synthesis may elucidate processes relevant to the origin, evolution, and distribution of life on Earth (Gontareva and Kuzicheva 2001). Complex organic molecules may have been formed via UV irradiation of icy grains in the solar nebula (Ciesla and Sandford 2012), as UV-irradiated ice analogs containing H_2O, CO, CO_2, NH_3, and CH_3OH produced a variety of organic molecules in laboratory simulations (Hagen et al. 1979). Surface-gas reactions may form organic molecules in the interstellar medium (ISM) (Ehrenfreund and Charnley 2000). Additionally, parent bodies of meteorites may provide conditions for

complex organic molecule formation through catalytic reactions on grain surfaces, e.g., Fischer–Tropsch reactions (Pizzarello and Shock 2000).

As for the extraterrestrial materials, there is evidence that indicates partial segregation of organic matter among specific minerals in heterogeneous meteorites. For instance, carbon chains were found to be longer when clays were present during laboratory prebiotic peptide synthesis (Paecht-Horowitz 1974). Additionally, kaolinite was found to be a more effective catalyst than montmorillonite for the production of amino acids from organic-kaolinite mixtures (Degens and Matheja 1971). Indeed, Hanafusa and Akabori (1959) pointed out the importance of clay minerals in condensation reactions, and showed that certain organic molecules form in the presence of kaolinite, but not in its absence. Furthermore, Pearson et al. (2002) reported that organic material was associated with clays but not with other hydrated mineral grains in CI and CM chondrites. Specifically, Pearson et al. (2002) reported that organics and clay minerals were found together on the chondrule rims of Murchison.

In this study, we investigated relationships of organic matter with inorganic material in NWA 852, and showed that aliphatic hydrocarbons are spatially correlated with both silicates and OH. This suggests that hydrated silicates are closely associated with organics in NWA 852. Therefore, our results indicate that such silicates may have played a catalytic role for production of organics in NWA 852.

NWA 852 is more primitive, i.e., less processed, than several other carbonaceous chondrites. Evidence from this and other work is as follows.

1. Presolar grain abundances are high in NWA 852 (Leitner et al. 2012), while parent-body processing by aqueous alteration and thermal metamorphism reduces such abundances (e.g., Trigo-Rodriguez and Blum 2009; Leitner et al. 2012; Zhao et al. 2013). For instance, abundances decrease in going from type 3 to type 1 carbonaceous chondrites, e.g., abundances are high in the CR3 chondrites Meteorite Hills (MET 00426) and Queen Alexandra Range (QUE 99177) (Floss and Stadermann 2009) and in IDPs (Messenger et al. 2003). This suggests that among CR2s, parent-body alteration for NWA 852 was less. In other words, NWA 852 lies closer to the CR3 side of the CR2 meteorite distribution, even though the presolar silicate-to-oxide ratio (~2) (Leitner et al. 2012), compared with CR3 chondrites (~22) (Floss and Stadermann 2009; Nguyen et al. 2010) and IDPs (~21) (Messenger et al. 2003, 2005), suggests aqueous alteration in NWA 852.
2. Bond breaking and chain shortening by energetic particles and thermal processing may lower CH_2/CH_3 ratios of aliphatic hydrocarbons (Merouane et al. 2012). NWA 852 has a relatively high ratio, although the broad spatial distribution of this ratio indicates some processing to higher or lesser degree in different parts.
3. Raman D and G band profiles for insoluble organic matter show that CR chondrites (which include NWA 852) are more primitive than CI and CM chondrites (e.g., Busemann et al. 2007). This is consistent with the high CH_2/CH_3 ratio for NWA 852 compared to CI and CM materials (Table 3).
4. NWA 852 lacks aromatic CH stretch bands above 3000 cm^{-1}, while aromatics have been observed in altered meteorites with low CH_2/CH_3 ratios, e.g., Murchison (Flynn et al. 2003) and Paris (Merouane et al. 2012).
5. CR chondrites are considered to contain the most primitive organic matter (Le Guillou and Brearley 2014).

NWA 852, IDPs (Keller et al. 2006), and Wild 2 cometary dust particles (Keller et al. 2006) all have similar aliphatic C-H stretching spectral features and CH_2/CH_3 ratios, whose values (~2.5) are more than twice larger than those for other primitive carbonaceous chondrites such as Orgueil and Murchison (~1.1) and for diffuse ISM objects (~1.2) (Table 3). This suggests different formation and/or parent body processing histories for these two groups of materials (Matrajt et al. 2005).

We believe that NWA 852 is (on average) on the low aqueous alteration side of petrologic type 2 with little thermal metamorphism. It would be useful to extend our technique to other meteorites to characterize the effects of parent body thermal metamorphism on the organic molecules and mineral species. In principle, our technique could deconvolve the imprints of thermal and aqueous alteration on the parent body from nebular signatures based on spatial distributions of spectral signatures: carbonates are secondary products that result from aqueous alteration, thermally metamorphosed material has little or no hydration, and a nebular signature is the high ratio of CH_2/CH_3. The question is whether regions of high CH_2/CH_3 ratio are spatially distinct from regions of high carbonates (altered) and regions of low hydration. In case of NWA 852, Table 2 suggests that carbonates are uncorrelated with aliphatic hydrocarbons ($r = 0.01$); however, this correlation is still uncertain due to the small number of observations ($n = 33$). We expect to see a stronger negative correlation in a larger data set for NWA 852.

Aqueous alteration may have redistributed the soluble organic material, which would tend to erase the mineralogical context of the organic molecules present. However, the *in*soluble fraction of organic matter

(IOM) ranges from 70 to 99% of the total in carbonaceous chondrites (Pizzarello et al. 2006; Kebukawa et al. 2011). Although there has been no report of the percent IOM in NWA 852, the soluble fraction is in any case a minority. Even then, Morlok and Libourel (2013) showed that dissolved elements stay close to their source in CR chondrites, and large organic molecules can be expected to be even less mobile through a solid matrix than are soluble elements. In highly altered grains, characteristic ~100 μm migration distances are two orders more than the length scale of spatial variations we observe in NWA 852, which agrees with its relatively low alteration. In other words, alteration in NWA 852 has not "washed out" the spatial heterogeneity of its organics.

IOM extracts may give different conclusions than in situ characterization such as ours. IOM is obtained by demineralizing the bulk sample in acidic solvents such as HF and HCl (e.g., Kebukawa et al. 2011; Orthous-Daunay et al. 2013). After demineralization, the remaining material is the IOM residue. Whether chemical alteration of organic matter through acidic demineralization occurs (Flynn et al. 2010; Matrajt et al. 2013), or not (Matrajt et al. 2005), is controversial. Flynn et al. (2010) showed that the Murchison IOM and in situ organic matter of bulk Murchison sample are significantly different. Chemical alteration effects include a decrease in the aliphatic CH_2/CH_3 ratios (giving shorter chains or more branching) and increase in aromatic CH content.

Another remaining question is whether organic abundances depend on grain size. We have demonstrated strong variations in organic concentrations over length scales of microns. At sufficiently small length scales, one expects eventually to find pure phases. Thus, a survey of very small grains (few microns) should exhibit large deviations in organic abundances from the meteorite average, from none to heavy concentrations.

Infrared transmittance spectroscopy requires thin specimens, so that the beam traverses only a few microns of matter to avoid saturating the strongest bands. This is most conveniently achieved by crushing the sample to obtain individual grains. Then, of course, some of the petrographic context is lost, i.e., we lose information on chemical and mineral distributions over length scales of several mm. We retain it on length scales of ~10 μm, and we can preserve it over length scales of several mm by crushing different samples from different portions of the parent meteorite.

Few reports exist on infrared spatial mapping of meteorites. For instance, Raynal et al. (2000) reported absorbance maps of Murchison and Orgueil using synchrotron-based FTIR microspectroscopy with comparatively low spatial resolution. Spatial mapping for a set of discrete wavelengths corresponding to different functional groups in Bells meteorite was presented by Kebukawa et al. (2010a), but abundances are more uncertain than those we obtain by integration over the full band widths spanned by those functional groups. For instance, our maps based on integrals over the full water absorbance spectral range 3000–3750 cm^{-1} should have less uncertainty than a map determined by the absorbance at (e.g.) the single wave number 3400 cm^{-1}. Furthermore, the near-field infrared microspectroscopy and spatial mapping by step scanning of Kebukawa et al. (2010a) is very slow in comparison to our approach. We presented infrared microspectroscopy of one grain of a CR2 chondrite NWA 852, demonstrating high spatial resolution and with high spectral information. We have also demonstrated chemically specific heterogeneity on 1 μm length scales.

CONCLUSION

We investigated relationships among organics and minerals in a CR2 chondrite NWA 852 by a highly novel analytical technique: midinfrared synchrotron-based imaging micro-FTIR spectroscopy. These data constitute the first reported infrared spectra for this meteorite. A spectroscopic line profile for the particular NWA 852 grain studied shows that the relative intensity of the characteristic absorbance bands varies across the grain on 1 μm length scales. Statistical analysis shows that silicates, OH, and CH are spatially correlated with each other. These correlations indicate a possible catalytic role of phyllosilicates for the formation of organic matter. However, the spatial overlap of silicate and OH is smaller, probably due to a heterogeneous mixture of anhydrous and hydrous silicates. The carbonate band is spatially anticorrelated with the water+organic band, however uncorrelated with any other spectral feature. Average CH_2/CH_3 ratio for NWA 852 indicates a predominance of CH_2 over CH_3 that is comparable to that in IDPs and Wild 2 cometary dust particles. The ratio significantly exceeds the CH_2/CH_3 ratio of DISM and several carbonaceous chondrites, indicating longer carbon chain lengths and/or smaller degree of branching. This may also indicate similar origin, formation, and/or processing of organic matter in NWA 852, IDPs, and Wild 2 particles, but rather different than diffuse ISM organic matter.

Acknowledgments—Mr. Yesiltas was primarily supported through Graduate Fellowship Program #1416 by the Turkish government. SRC was primarily funded by the University of Wisconsin-Madison with supplemental

support from facility users and the University of Wisconsin-Milwaukee. IRENI beamline's construction and development was supported by NSF MRI award # 0619759, and CJH was funded by NSF CHE award # 1112433. We thank Prof. Daniel Britt and Prof. Humberto Campins for critically reading the manuscript and making a number of valuable suggestions. We are also grateful to associate editor Dr. G. Benedix and anonymous reviewers for constructive comments on this manuscript.

Editorial Handling—Dr. Gretchen Benedix

REFERENCES

Anders E. 1975. Do stony meteorites come from comets? *Icarus* 24:363–371.

Beck P., Quirico E., Montes-Hernandez G., Bonal L., Bollard J., Orthous-Daunay F. R., Howard K. T., Schmitt B., Brissaud O., Deschamps F., Wunder B., and Guillot S. 2010. Hydrous mineralogy of CM and CI chondrites from infrared spectroscopy and their relationship with low albedo asteroids. *Geochimica et Cosmochimica Acta* 74:4881–4892.

Botta O. and Bada J. L. 2002. Extraterrestrial organic compounds in meteorites. *Surveys in Geophysics* 23:411–467.

Briani G., Quirico E., Gounelle M., Paulhiac-Pison M., Montagnac G., Beck P., Orthous-Daunay F. R., Bonal L., Jacquet E., Kearsley A., and Russell S. S. 2013. Short duration thermal metamorphism in CR chondrites. *Geochimica et Cosmochimica Acta* 122:267–279.

Brown P. G., Hildebrand A. R., Zolensky M. E., Grady M., Clayton R. N., Mayeda T. K., Tagliaferri E., Spalding R., MacRae N. D., Hoffman E. L., Mittlefehldt D. W., Wacker J. F., Bird A., Campbell M. D., Carpenter R., Gingerich H., Glatiotis M., Greiner E., Mazur M. J., McCausland P. J., Plotkin H., and Mazur T. R. 2000. The fall, recovery, orbit, and composition of the Tagish Lake meteorite: A new type of carbonaceous chondrite. *Science* 290:320–325.

Busemann H., Alexander C. M. O'D., and Nittler L. R. 2007. Characterization of insoluble organic matter in primitive meteorites by microRaman spectroscopy. *Meteoritics & Planetary Science* 42:1387–1416.

Campins H., Hargrove K., Pinilla-Alonso N., Howell E. S., Kelley M. S., Licandro J., Mothe-Diniz T., Fernandez Y., and Ziffer J. 2010. Water ice and organics on the surface of the asteroid 24 Themis. *Nature* 464:1320–1321.

Chyba C. and Sagan C. 1992. Endogenous production, exogenous delivery and impact-shock synthesis of organic molecules—An inventory for the origins of life. *Nature* 355:125–132.

Ciesla F. J. and Sandford S. A. 2012. Organic synthesis via irradiation and warming of ice grains in the solar nebula. *Science* 336:452–45.

Cleaves J. H., Michalkova S. A., Hill F. C., Leszczynski J., Sahai N., and Hazen R. 2012. Mineral-organic interfacial processes: Potential roles in the origins of life. *Chemical Society Reviews* 41:5502–5525.

Cloutis E. A., Hudon P., Hiroi T., and Gaffey M. J. 2012. Spectral reflectance properties of carbonaceous chondrites: 3. CR chondrites. *Icarus* 217:389–407.

Cohen J. 1988. *Statistical power analysis for the behavioral sciences*, 2nd edn. Hillsdale, New Jersey: Erlbaum.

Degens E. T. and Matheja J. 1971. Formation of organic polymers on inorganic templates. In *Prebiotic and biochemical evolution*, edited by Kimball A. P. and Oro J. Amsterdam: North Holland. pp. 39–69.

Désaubry L., Nakatani Y., and Ourisson G. 2003. Toward higher polyprenols under "prebiotic conditions". *Tetrahedron Letters* 44:6959–6961.

Ehrenfreund P. and Charnley S. B. 2000. Organic molecules in the interstellar medium, comets, and meteorites: A voyage from dark clouds to the early Earth. *Annual Review of Astronomy and Astrophysics* 38:427–483.

Floss C., and Stadermann F. 2009. High abundances of circumstellar and interstellar C-anomalous phases in the primitive CR3 chondrites QUE 99177 and MET 00426. *The Astrophysical Journal* 697:1242–1255.

Flynn G. J., Keller L. P., Feser M., Wirick S., and Jacobsen C. 2003. The origin of organic matter in the solar system: Evidence from the interplanetary dust particles. *Geochimica et Cosmochimica Acta* 67:4791–4806.

Flynn G. J., Wirick S., Keller L. P., and Jacobsen C. 2010. Modification of the Murchison insoluble organic matter (IOM) by acid extraction (abstract #5162). LPI Contribution 1538. Houston, Texas: Lunar and Planetary Institute. 5162 p.

Gontareva N. B., and Kuzicheva E. A. 2001. Laboratory photochemical formation of peptides in presence of meteorites as a model of chemical evolution process. Proceedings of the First European Workshop. pp. 345–348.

Hagen W., Allamandola L. J., and Greenberg J. M. 1979. Interstellar molecule formation in grain mantles: The laboratory analog experiments, results and implications. *Astrophysics and Space Science* 65:215–240.

Hanafusa H. and Akabori S. 1959. Polymerization of aminoacetonitrile. *Bulletin of the Chemical Society of Japan* 32:626–630.

Hirschmugl C. J. and Gough K. M. 2012. Fourier transform infrared spectrochemical imaging: Review of design and applications with a focal plane array and multiple beam synchrotron radiation source. *Applied Spectroscopy* 66:475–491.

Hopkins K. D. 1978. *Basic statistics for the behavioral sciences*. Englewood Cliffs, New Jersey: Prentice-Hall Inc.

Huss G. R., Rubin A. E., and Grossman J. N. 2006. Thermal metamorphism in chondrites. In *Meteorites and the early solar system II*, edited by Lauretta D. and McSween H. Y. Jr. Tuscon, AZ: The University of Arizona Press. pp. 567–586.

Igisu M., Ueno Y., Shimojima M., Nakashima S., Awramik S. M., Ohta H., and Maruyama S. 2009. Micro-FTIR spectroscopic signatures of bacterial lipids in proterozoic microfossils. *Precambrian Research* 173:19–26.

Kebukawa Y., Nakashima S., Otsuka T., Nakamura-Messenger K., and Zolensky M. E. 2009. Rapid contamination during storage of carbonaceous chondrites prepared for micro FTIR measurements. *Meteoritics & Planetary Science* 44:545–557.

Kebukawa Y., Nakashima S., Ishikawa M., Aizawa K., Inoue T., Nakamura-Messenger K., and Zolensky M. E. 2010a. Spatial distribution of organic matter in the Bells CM2

chondrite using near-field infrared microspectroscopy. *Meteoritics & Planetary Science* 45:394–405.

Kebukawa Y., Nakashima S., and Zolensky M. E. 2010b. Kinetics of organic matter degradation in the Murchison meteorite for the evaluation of parent-body temperature history. *Meteoritics & Planetary Science* 45:99–113.

Kebukawa Y., Alexander C. M. O'D., and Cody G. D. 2011. Compositional diversity in insoluble organic matter in type 1, 2 and 3 chondrites as detected by infrared spectroscopy. *Geochimica et Cosmochimica Acta* 75:3530–3541.

Keller L. P., Bajt S. A., Baratta G. A., Borg J., Bradley J. P., Brownlee D. E., Busemann H., Brucato J. R., Burchell M., Colangeli L., d'Hendecourt L., Djouadi Z., Ferrini G., Flynn G., Franchi I. A., Fries M., Grady M. M., Graham G. A., Grossemy F., Kearsley A., Matrajt G., Nakamura-Messenger K., Mennella V., Nittler L., Palumbo M. E., Stadermann F. J., Tsou P., Rotundi A., Sandford S. A., Snead C., Steele A., Wooden D., and Zolensky M. 2006. Infrared spectroscopy of comet 81P/Wild 2 samples returned by Stardust. *Science* 314:1728–1731.

Lahav N. and Chang S. 1976. The possible role of solid surface area in condensation reactions during chemical evolution: Reevaluation. *Journal of Molecular Evolution* 8:357–380.

Le Guillou C. and Brearley A. J. 2014. Relationships between organics, water and early stages of aqueous alteration in the pristine CR3.0 chondrite MET 00426. *Geochimica et Cosmochimica Acta* 131:344–367.

Leitner J., Vollmer C., Hoppe P., and Zipfel J. 2012. Characterization of presolar material in the CR chondrite Northwest Africa 852. *The Astrophysical Journal* 745:38–53.

Licandro J., Campins H., Kelley M., Hargrove K., Pinilla-Alonso N., Cruikshank D., Rivkin A. S., and Emery J. 2011. (65) Cybele: detection of small silicate grains, water-ice, and organics. *Astronomy & Astrophysics* 525:A34.

Marshall C. P., Javaux E. J., Knoll A. H., and Walter M. R. 2005. Combined micro-Fourier transform infrared (FTIR) spectroscopy and micro-Raman spectroscopy of proterozoic acritarchs: A new approach to palaeobiology. *Precambrian Research* 138:208–224.

Martins Z. 2011. Organic chemistry of carbonaceous meteorites. *Elements* 7:35–40.

Matrajt G., Borg J., Raynal P. I., Djouadi Z., d'Hendecourt L., Flynn G., and Deboffle D. 2004. FTIR and Raman analyses of the Tagish Lake meteorite: Relationship with the aliphatic hydrocarbons observed in the diffuse interstellar medium. *Astronomy & Astrophysics* 416:983–990.

Matrajt G., Muñoz Caro G., Dartois E., d'Hendecourt L., Deboffle D., and Borg J. 2005. FTIR analysis of the organics in IDPs: Comparison with the IR spectra of the diffuse interstellar medium. *Astronomy & Astrophysics* 433:979–995.

Matrajt G., Flynn G., Brownlee D., Joswiak D., and Bajt S. 2013. The origin of the 3.4 μm feature in Wild 2 cometary particles and in ultracarbonaceous interplanetary dust particles. *The Astrophysical Journal* 765:145.

Merouane S., Djouadi Z., d'Hendecourt L. L. S., Zanda B., and Borg J. 2012. Hydrocarbon materials of likely interstellar origin from the Paris meteorite. *The Astrophysical Journal* 756:154.

Messenger S., Keller L. P., Stadermann F. J., Walker R. M., and Zinner E. 2003. Samples of stars beyond the solar system: Silicate grains in interplanetary dust. *Science* 300:105–108.

Messenger S., Keller L. P., and Lauretta D. S. 2005. Supernova olivine from cometary dust. *Science* 309:737–741.

Morbidelli A., Chambers J., Lunine J. I., Petit J. M., Robert F., Valsecchi G. B., and Cyr K. E. 2000. Source regions and timescales for the delivery of water to the Earth. *Meteoritics & Planetary Science* 35:1309–1320.

Morlok A. and Libourel G. 2013. Aqueous alteration in CR chondrites: Meteorite parent body processes as analogue for long-term corrosion processes relevant for nuclear waste disposal. *Geochimica et Cosmochimica Acta* 103:76–103.

Nakamura K., Nakashima S., Tomita S., Zolensky M. E., Keller L. P., and Tomeoka K. 2003a. Hollow organic globules in the Tagish Lake meteorite as possible products of primitive organic reactions. *Geochimica et Cosmochimica Acta* 67:A325–A325.

Nakamura T., Noguchi T., Zolensky M. E., and Tanaka M. 2003b. Mineralogy and noble-gas signatures of the carbonate-rich lithology of the Tagish Lake carbonaceous chondrite: Evidence for an accretionary breccia. *Earth and Planetary Science Letters* 207:83–101.

Nasse M. J., Mattson E. C., Reininger R., Kubala T., Janowski S., El-Bayyari Z., and Hirschmugl C. J. 2011. Multi-beam synchrotron infrared chemical imaging with high spatial resolution: Beamline realization and first reports on image restoration. *Nuclear Instruments and Methods in Physics Research Section A: Accelerators, Spectrometers, Detectors and Associated Equipment* 649:172–176.

Nguyen A. N., Nittler L. R., Stadermann F. J., Stroud R. M., and Alexander C. M. O'D. 2010. Coordinated analysis of presolar grains in the Allan Hills 77307 and Queen Elizabeth Range 99177 meteorites. *The Astrophysical Journal* 719:166–189.

Orthous-Daunay F. R., Quirico E., Beck P., Brissaud O., Dartois E., Pino T., and Schmitt B. 2013. Mid-infrared study of the molecular structure variability of insoluble organic matter from primitive chondrites. *Icarus* 223:534–543.

Owen T. and Bar-Nun A. 1995. Comets, impacts, and atmospheres. *Icarus* 116:215–26.

Paecht-Horowitz M. 1974. The possible role of clays in prebiotic peptide synthesis. *Origins of Life* 5:173–187.

Pearson V. K., Sephton M. A., Kearsley A. T., Bland P. A., Franchi I. A., and Gilmour I. 2002. Clay mineral-organic matter relationships in the early solar system. *Meteoritics & Planetary Science* 37:1829–1833.

Pendleton Y., Sandford S., Allamandola L., Tielens A., and Sellgren K. 1994. Near-infrared absorption spectroscopy of interstellar hydrocarbon grains. *The Astrophysical Journal* 437:683–696.

Pizzarello S. and Shock E. 2000. The organic composition of carbonaceous meteorites: The evolutionary story ahead of biochemistry. *Cold Spring Harbor Perspectives in Biology* 2:a002105. doi:10.1101/cshperspect.a002105.

Pizzarello S., Cooper G. W., and Flynn G. J. 2006. The nature and distribution of the organic material in carbonaceous chondrites and interplanetary dust particles. In *Meteorites and the early solar system II*, edited by Lauretta D. S. and McSween H. Y. Jr. Tuscon, Arizona: The University of Arizona Press. pp. 625–651.

Ponnamperuma C., Shimoyama A., and Friebele E. 1982. Clay and the origin of life. *Origins of Life and Evolution of the Biosphere* 12:9–40.

Raynal P. I., Quirico E., Borg J., Deboffle D., Dumas P., d'Hendecourt L., Bibring J. P., and Langevin Y. 2000. Synchrotron infrared microscopy of micron-sized extraterrestrial grains. *Planetary and Space Science* 48:1329–1339.

Rivkin A. S. and Emery J. P. 2010. Detection of ice and organics on an asteroidal surface. *Nature* 464:1322–1323.

Rode B. M., Son H. L., Suwannachot Y., and Bujdak J. 1999. The combination of salt induced peptide formation reaction and clay catalysis: A way to higher peptides under primitive earth conditions. *Origin of Life and Evolution of the Biosphere* 29:273–286.

Russell S. S., Zipfel J., Grossman J. N., and Grady M. M. 2002. The Meteoritical Bulletin, No. 86. *Meteoritics and Planetary Science* 37:A157–A184.

Sandford S., Allamandola L., Tielens A., Sellgren K., Tapia M., and Pendleton Y. 1991. The interstellar CH stretching band near 3.4 microns—Constraints on the composition of organic material in the diffuse interstellar medium. *The Astrophysical Journal* 371:607–620.

Sandford S., Nuevo M., Flynn G., and Wirick S. 2013. Mid-infrared study of samples from several stones from the Sutter's Mill meteorite (abstract #1663). 44th Lunar and Planetary Science Conference. CD-ROM.

Sephton M. A. 2002. Organic compounds in carbonaceous meteorites. *Natural Product Reports* 19:292–311.

Sephton M. A., Pillinger C. T., and Gilmour I. 1998. delta(13) C of free and macromolecular aromatic structures in the Murchison meteorite. *Geochimica et Cosmochimica Acta* 62:1821–1828.

Sephton M. A., Verchovsky A. B., Bland P. A., Gilmour I., Grady M. M., and Wright I. P. 2003. Investigating the variations in carbon and nitrogen isotopes in carbonaceous chondrites. *Geochimica et Cosmochimica Acta* 67:2093–2108.

Trigo-Rodriguez J. M. and Blum J. 2009. The effect of aqueous alteration and metamorphism in the survival of presolar silicate grains in chondrites. *Publications of the Astronomical Society of Australia* 26:289–296.

Vernazza P., Carry B., Emery J., Hora J., Cruikshank D., Binzel R., Jackson J., Helbert J., and Maturilli A. 2010. Mid-infrared spectral variability for compositionally similar asteroids: Implications for asteroid particle size distributions. *Icarus* 207:800–809.

Yesiltas M., Hirschmugl C., and Peale R. 2013a. In situ investigation of meteoritic organic-mineral relationships by high spatial resolution infrared spectroscopy (abstract #5068). *Meteoritics & Planetary Science* 48.5068.pdf.

Yesiltas M., Unger M., Sedlmair J., Hirschmugl C., Brusentsova T., Arnold J., and Peale R. 2013b. Microspectroscopy of meteorites: Search for organic-mineral correlations (abstract #2717). 44th Lunar and Planetary Science Conference. CD-ROM.

Yesiltas M., Kebukawa Y., Peale R. E., Mattson E., Hirschmugl C. J., and Jenniskens P. 2014. Infrared imaging spectroscopy with micron resolution of Sutter's Mill meteorite grains. *Meteoritics & Planetary Science* 49:2027–2037.

Zhao X., Floss C., Lin Y., and Bose M. 2013. Stardust investigation into the CR chondrite Grove Mountain 021710. *The Astrophysical Journal* 769:49.